Title

Highly Flexible Wrinkled Carbon Nanotube Thin Film Strain Sensor to Monitor Human Movement



Journal

Advanced Materials Technologies, 1(2)

Authors

Park, S-J

Kim, J

Chu, M

et al.

Publication Date

2023-12-10

ADVANCED MATERIALS TECHNOLOGIES
www.advmattechnol.de



# Highly Flexible Wrinkled Carbon Nanotube Thin Film Strain Sensor to Monitor Human Movement

*Sun-Jun Park, Joshua Kim, Michael Chu, and Michelle Khine**

There is a growing need to improve the mechanical reliability of flexible electronics as the demand for 'wearable' applications in health and medical monitoring increases. These new wearable electrical components must conform to soft curvilinear surfaces, stretch and flex with the body's motion, and be lightweight and unobtrusive. It is critical to overcome rigid, brittle, and largely planar electronics and sensors to develop more insightful investigations for human body monitoring.[1,2] Thus, flexible electronics will fulfill the growing interest in long term monitoring systems for personalized fitness, physical rehabilitation, finger sensing microswitches, entertainment devices, and continuous health monitoring for various parameters such as blood pressure, breathing and body temperature.[3–9]

Wearable strain sensor devices are designed to be mounted on the human skin to measure the strain induced by muscle movements. Many sensors transduce the mechanical deformation to a resistance change upon stretching and releasing. This phenomenon is known as the piezoresistive effect. The relative change in resistance, $\Delta R/R_0$, is related to the mechanical strain $\varepsilon$ by the gauge factor (GF) according to Equation (1)[1]

$$\mathrm{GF} = \frac{\Delta R/R_0}{\varepsilon} \tag{1}$$

In order to be an effective strain sensor for monitoring human motion, the sensors must have high flexibility and stretchability, while maintaining sensitivity across a large dynamic range. For example, high gauge factor strain sensors are able to measure both small and large angle deformations inherent to human joint motion. Thus, there has been a large amount of research in developing highly stretchable and sensitive wearable strain sensors by using micro/nanostructured thin films, functional materials, and elastomeric substrates.

Micro- and nanostructures have been implemented by researchers to improve the elasticity of brittle materials.[10–12] These micro/nanostructures are typically generated via buckling from compressive substrates. For example, researchers have deposited brittle materials onto pre-strained silicon rubbers and released the strain to create wavy buckled structures. These wavy buckled structures provided strain relief for brittle materials rendering them stretchable.[13,14]

Typical wearable strain sensors consist of patterned thin films on flexible elastomeric substrates. Recent developments in creating highly stretchable wearable strain sensors used nanoscale metal thin films,[15] nanoparticles,[16] nanowires (NWs),[17–19] nanotubes,[20–26] and graphene.[27–31] For example, Kang et al. utilized brittle platinum thin films to achieve high sensitivity (GF > 2000), but the strain sensor was only able to withstand strains of up to 2%.[32] Li et al. investigated graphene woven fabric for strain sensing (GF ≈ 1000), but was still limited to a maximum strain of 6%.[33] Conversely, Yan et al. reported highly stretchable graphene-nanocellulose nanopaper that can stretch out to 100% strain, but the strain sensor only had a GF of 7.1.[34] Zaretski et al. reported a highly sensitive strain sensor using metallic nanoislands on graphene with GF 1335 at 1% strain. However, the dynamic range of this sensor was limited, with strain of less than 10% strain. Additionally, the GF dropped to 743 after 19 cycles at 1% strain.[35]

Another popular functional material that is used for strain sensing is carbon nanotubes (CNTs). Percolating networks of CNTs on flexible elastomeric substrates have been reported to have electromechanical stability under high strain due to the robust contact between individual CNTs.[36] CNT thin films have also shown the ability to bend repeatedly without fracturing.[37–41] Therefore, percolating networks of CNTs have the potential to be used as highly stretchable strain sensing devices. For instance, Yamada et al. aligned CNT thin film on PDMS and showed 280% strain but low sensitivity (GF < 0.82),[25] and Lipomi et al. investigated spring like structures in the nanotube that reach 150% strain with good conductivity.[22] Ryu et al. showed that aligned CNT fibers grown on flexible substrates were able to stretch out to 900% having GF of up to 47.[42] However, this process required highly ordered alignment of CNT fibers using intricate dry spinning methods.

Another aspect to consider for improving wearable strain sensor is the careful selection of the stretchable elastomeric substrate. Many strain sensors have been fabricated using polydimethylsiloxane (PDMS) as the stretchable and flexible substrate due to its flexibility, nontoxicity, ease of fabrication, and biocompatibility.[43,44] Amjadi et al. reported highly flexible, stretchable sensitive strain sensors based on silver nanowires with PDMS that had a GF of 14 at 70% strain.[44] However, many PDMS substrate based strain sensors showed low stretchability with high hysteresis due to poor adhesion between the functional material and substrate polymer, as well as increased friction during the strain.[45,46] Furthermore, PDMS becomes stiffer, delaminates, and slips after absorbing human sweat

S.-J. Park, J. Kim, Prof. M. Khine
Department of Chemical Engineering
and Materials Science
University of California Irvine
Irvine, CA 92697, USA
E-mail: mkhine@uci.edu
M. Chu, Prof. M. Khine
Department of Biomedical Engineering
University of California Irvine
Irvine, CA 92697, USA

DOI: 10.1002/admt.201600053

and moisture. Finally, the Young's moduli mismatch between PDMS (0.4–3.5 MPa) and the human skin (25–220 kPa) induces more stress into the strain sensor, and even more so when integrated with thin films such as CNT, Ag, Au, and Si.[43,47–50]

There have been recent efforts to mimic the properties of the human skin more accurately by using Ecoflex, a platinum-catalyzed elastic silicone material. Ecoflex has a Young's modulus of ≈125 kPa, similar to that of human epidermis.[51] Second, it can stretch and withstand strains greater than 900% and rebounds back to its initial size without tearing and distortion. Third, it is highly water resistant allowing for long term wear on the human body. Lastly, Ecoflex is biocompatible, nontoxic, and FDA approved. Therefore, Ecoflex is a more suitable candidate for wearable strain sensors.

In this paper, we introduce a scalable and simple method to fabricate wearable strain sensors with self-similar nano- to microsized wrinkled CNT thin film in Ecoflex. We have previously demonstrated that self-similar hierarchal wrinkled structures in metal thin films can be created via heat induced biaxial shrinking on shape memory polymers (SMPs), such as polystyrene(PS).[52] The buckling occurs due to the mismatches in stiffness between the SMP and the deposited material during the shrinking process.[53] Spray gun deposition was used to deposit CNT thin films on SMP. The spray gun deposition method is known to be simple, cost-effective and fast. Spray gun deposition has already been adopted as a scalable process used to uniformly deposit thin films, such as CNTs.[54,55] Spray gun deposition and the use of SMP makes our fabrication process scalable, simple, and quick compared to other CNT based strain sensors methods. Here we demonstrate that mats of deposited CNTs on the SMP result in densified, self-similar nano- to microfeatured wrinkles upon shrinkage. We show that these wrinkled CNT thin films can be transferred from the rigid SMP carrier film into Ecoflex 0030. (Smooth-On, PA). The tight entangled CNTs introduce strong van der Waals forces between CNTs to enhance stretchability. Furthermore, these hierarchal self-similar wrinkled structures provide large amounts of strain relief during stretching. To our knowledge, this is the first demonstration of wrinkled CNT thin films fabricated using SMPs, which were integrated in a stretchable human motion sensor.

The fabrication process for self-similar wrinkled CNT-Ecoflex (wCE) strain sensors can be seen in **Figure 1**. A spray gun was used to deposit CNTs through a shadow mask and onto a PS substrate. We used a 0.5 mm diameter atomizing nozzle and

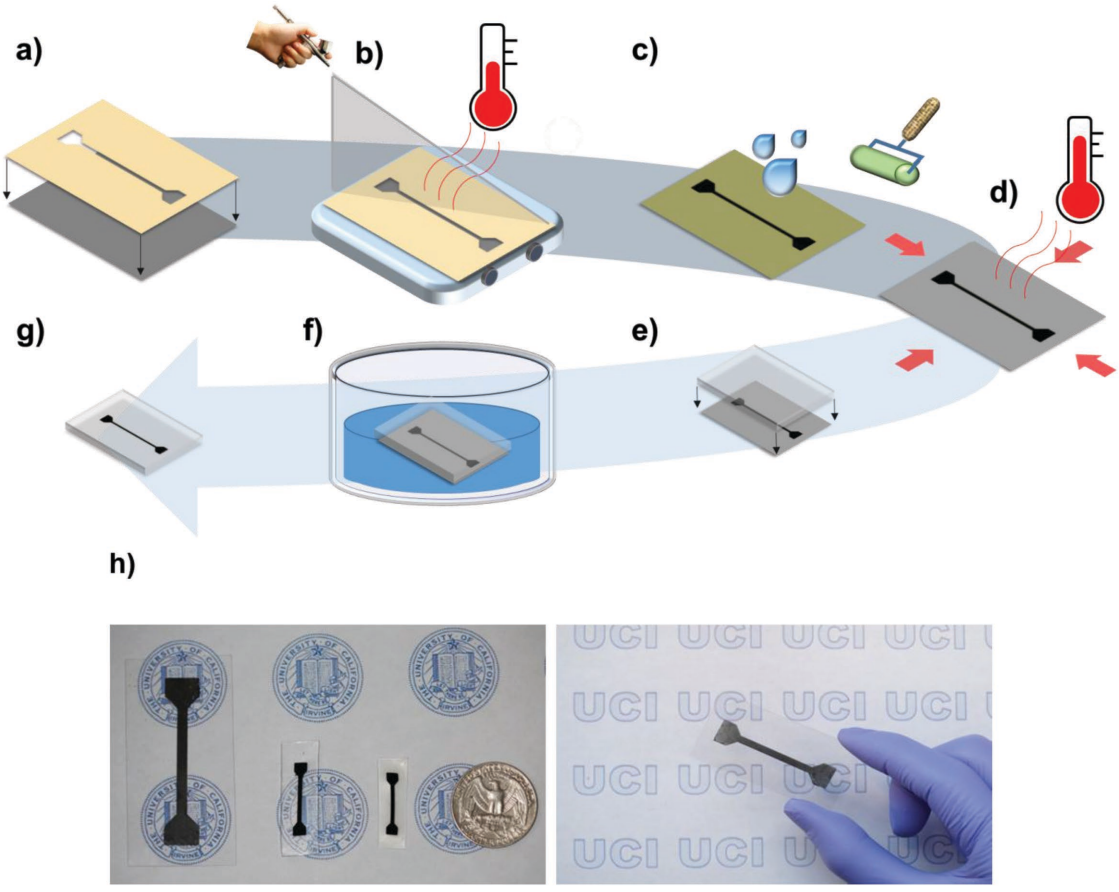


**Figure 1.** Fabrication process of self-similar wrinkles CNT-Ecoflex strain sensor. a) Shadow mask is attached onto PS substrate. b) Spray gun is used to deposit CNT thin film. c) Substrate was rinsed with deionized water and applied with pressure from a roller. d) Heat was applied to induce biaxial shrinking. e) Ecoflex was cured on shrunken PS substrate. f) Organic solvent bath was used to complete transfer process. g) Final self-similar wrinkled CNT thin film on Ecoflex substrate. h) Photograph of the CNT thin film at each step of the fabrication process: As deposit, shrunken, transferred (left), and CNT thin film on PS substrate (right).

pressures below 0.5 bar for the deposition of the CNT thin film. The thickness of the CNT thin film was easily controlled by the number of spray depositions on the substrate. After the spray deposition, the patterned CNT thin film was rinsed with deionized water and dried. After removing the patterned shadow mask, a paint roller was used to press against the CNT thin film to make the thin film denser. This step was performed to prevent the CNT network from embedding into the PS during heat induced shrinking. The sample was then placed into a convection oven set at 150 °C to induce biaxial shrinking and wrinkling of the CNT thin film. After shrinking, the sensor is about 33%–40% of the original size. After shrinking, Ecoflex was spun on top the sample and cured overnight at room temperature. The cured sample was then placed into an acetone bath followed by a toluene bath to transfer the wrinkled CNT thin film onto Ecoflex.

**Figure 2** shows scanning electron microscope images of the CNT thin film at different stages of the fabrication process. As deposited planar CNT thin film on PS is shown in Figure 2a. After heat induced shrinkage, the CNT thin film buckled and created self-similar wrinkled structures similar to those previously shown in metal thin films.[56] The CNT thin films wrinkle because each individual CNT is entangled and weakly adhered to each other via van der Waal forces resulting in one thin film as opposed to an assortment of individual CNTs. Scanning electron microscopy (SEM) images in the right-hand column of Figure 2 show that these wrinkled structures are comprised of individual CNTs. As seen in Figure 2c, the wrinkled structures were maintained after transferring into the soft silicone elastomer, Ecoflex. However, the shape of the wrinkles slightly changed due to swelling and shrinking of the Ecoflex during the organic solvent transfer process. The overall shape of the self-similar wrinkled structures was maintained. These self-similar wrinkled structures supported by a soft silicone elastomer allow the CNT thin film to become highly elastic.

**Figure 3** shows the stretching apparatus for straining and the strain-resistance behavior of self-similar wrinkled CNT thin films. As seen in Figure 3, wCE strain sensors were able strain

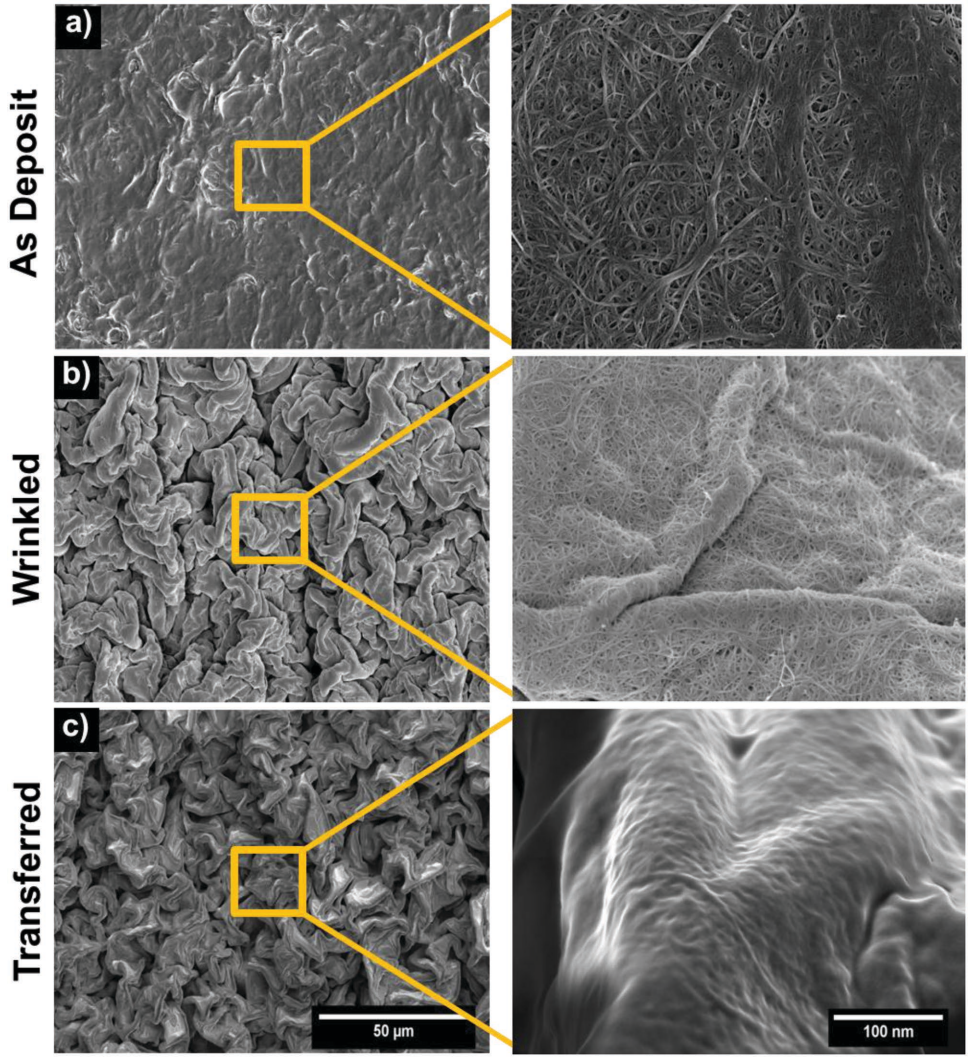


**Figure 2.** Scanning electron microscope images of the wrinkled CNTs. a) As deposited CNT thin film on PS substrate. b) Wrinkled CNT thin film on shrunken PS substrate. c) Transferred wrinkled CNT thin film on Ecoflex substrate. Left-hand column scale bar is 50 um and the inset's is 100 nm.

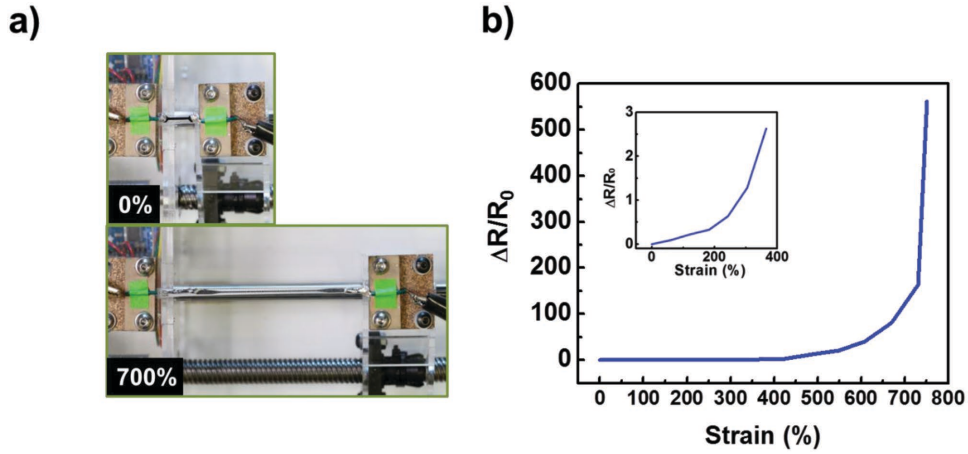


**Figure 3.** a) Image of a strain sensor at the initial length and stretched to 700% strain. b) Relative change in resistance vs strain on wrinkled CNTs on Ecoflex substrate (the inset plot is an expanded view of 0–400% strain)

out to ≈750% and remain conductive. On the contrary, planar CNT thin films (the control) were only able to stretch out to ≈12% (Supporting Information Figure S1). Therefore, the wrinkled structures provided a > 60 fold increase in stretchability. The reproducibility for the strain resistance behavior is shown in Figure S2 (Supporting Information).

The strain-resistance plot shows two distinct regions of strain: 0%–400% and 400%–700%. In the first region from 0%–400% strain, the relative change in resistance increased by a factor of 2.5 and the GF was 0.65. For this region, the change in electrical resistance is a combination of different factors. Predominantly, it is due to the increasing separation of neighboring wrinkled CNT structures and from the increase in the length of the wrinkle's geometry when stretched. Additionally, there is also a decrease in the effective cross-section area between CNTs and a separation of the individual CNTs by a van der Waals separation distance. This distance change between neighboring CNTs promotes an increase in the tunneling resistance. There may also be deformation of the individual CNTs themselves, which will increases the resistance of the tubes.[10,57–60] The second region from strains 400%–700%, the relative change in resistance increased by a factor of 162 and had a GF of 48. In this region, the CNT thin film started to fracture at strains greater than 400% as evidenced from the discontinuities and gaps within the thin film (Figure S3, Supporting Information). This reduces the number of conductive pathway so the relative change in resistance very large. Finite Element Analysis (FEA) of a 2D cross section show that the normal stress is localized within the valleys of the wrinkles during strain.[61,62] Furthermore, within each valley, the normal stress is highest at the top of the CNT thin film, CNT-Air interface, and lowest at the CNT-Ecoflex interface (Figure S4, Supporting Information).[48] As the model suggests, these localized stress points are most likely where the fractures nucleate. Within each valley, the fractures will propagate downward toward the CNT-Ecoflex interface. Throughout the entire film, these fractures expand to form a mesh like pattern of conductive pathways, similar to that of metal thin films.[63] The reduction of conductive pathways results in high resistance changes and subsequent high sensitivity in the second region.

The geometry of the elastomeric substrates also affects the performance of the wCE strain sensors. FEA of three different geometries (rectangular, dumbbell, and hourglass) shows that the shape affects the strain distribution throughout the Ecoflex during stretching. (Figure S5, Supporting Information) The FEA of the rectangular shaped elastomeric substrates showed the most uniform strain distribution, while the dumbbell and hourglass shaped geometries showed more localized strain in the center. This nonuniformity may result in earlier fracturing of the sensor in areas of higher strain concentration. Therefore, the rectangular geometry was chosen for the sensor because it maintains uniform strain along the longitudinal direction of the sensor. The uniform strain should help increase strain by uniformly distributing the fracture that occurs, minimizing the chance for a large discontinuity to form.

**Figure 4**. illustrates how incremental tensile strains, up to 750%, affect the CNT wrinkled structures. At 100% of strain, the CNT wrinkles started to align in the direction of the load. This is due to the compressive strains from the Ecoflex, which follows a positive Poisson ratio. The wrinkle structures completely aligned uniaxially at strains greater than 400%. After this point, the wrinkled structures were not able to provide any more strain relief resulting in fracture nucleation and propagation. Although the wrinkles were completely aligned, additional strain relief came from the percolating network of CNTs. At 750% strain, the fractures propagated completely across the trace resulting in sensor failure.

The response of the wCE strain sensor during a 300% cyclic strain can be seen in **Figure 5**. The normalized change in resistance was approximately 175% which corresponds well with Figure 3b. At 300% strain there was 145% change in resistance similar to that of the cyclic strain. This shows that the wCE sensor were robust after cyclic strain. Cyclic strains of 300% and 500% strain for 1000 cycles are shown in Figures S6 and S7 (Supporting Information). In addition to cyclic strain, the hysteresis responses for the wrinkled CNT-Ecoflex strain sensors at 100% and 300% strain were measured (Figure 5b). After releasing from 100% strain, there was a slight hysteresis showing a 1% change of resistance. Releasing at 300% strain,

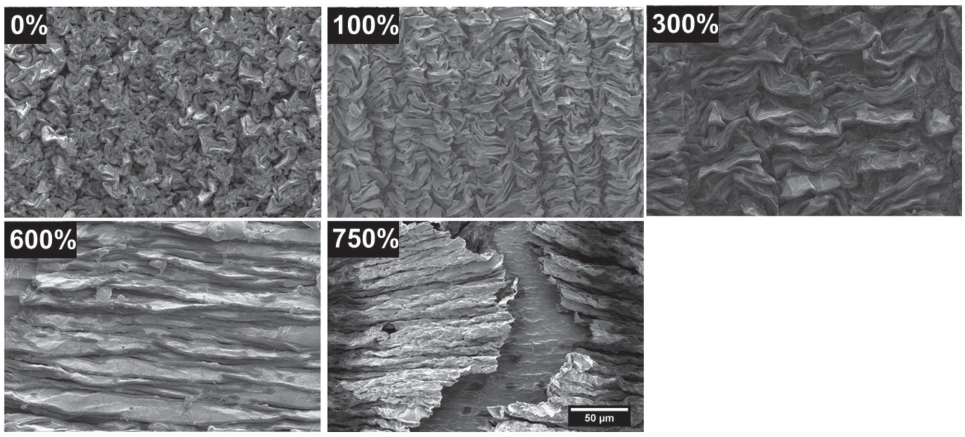


**Figure 4.** Scanning electron microscope images of the wrinkled CNT thin film on Ecoflex at different strains.

there was a 7% change of resistance due to the viscoelastic properties of the Ecoflex substrate.

To demonstrate the potential and applicability of the wCE sensor as a wearable device, the strain sensor was mounted on the elbow, knee, and finger to monitor their motion. The wCE sensor was assembled on an elastic sports fitness tape, KT Tape (KT Health (**Figure 6**c inset)). The wCE sensor was attached on the respective joints for the elbow, knee, and finger. (Figure 6). To measure the movement of the elbow, the initial elbow position was held flat and measurements were taken while the elbow was bent toward the body and returned back to the initial position. During the bending motion, the wCE sensor stretched and bent with the joint causing the relative change in resistance to increase. When returned back to the original position, the relative change of resistance returned back to baseline. The maximum strain for the elbow bending was 180%. To measure the bending motion of the knee, the sensor was attached on the knee cap and measurements were taken for a squatting motion. The knee was initially straight and then bent during the squatting motion. With a squat position, the sensor bended and stretched, and its relative change of resistance increased up to 230% strain. When returning back to the original position, relative resistance again decreased with the releasing of sensor. Lastly, measurements were made on the middle joint of the index finger at successive bending of 30°, 60°, and 90° (Figure 6c). The relatively change in resistance increased with increased bending and stretching. The measured relative changes in resistance were ≈17%, 24%, and 33%, respectively. The abovementioned experiments highlight the potential use of CNT–Ecoflex nanocomposite based strain sensors as an epidermal device for human skin motion detection.

In conclusion, we have introduced a new route to develop ultra-stretchable, human skin mountable, and sensitive strain sensor with low cost and simple fabrication procedure by forming stretchable wrinkled CNT networks. We have also demonstrated that wrinkled CNT networks can be transferred onto soft stretchable elastomeric substrates such as Ecoflex, while maintaining the self-similar nano- and microstructures and conductivity. Different sizes and wavelengths of wrinkles can be produced by depositing different thicknesses of the CNT solution. The feature size of the CNT wrinkle increases with the film thickness (Figure S8, Supporting Information). Furthermore, by uniaxial shrinking, the CNT wrinkle waves can alternatively align into one direction (Figure S9, Supporting Information). Our fabrication method is compatible with conventional and scalable manufacturing methods as previously reported.[54,55,64] The wCE sensor can measure up to ≈750% strain with high sensitivity. Finally, we demonstrate

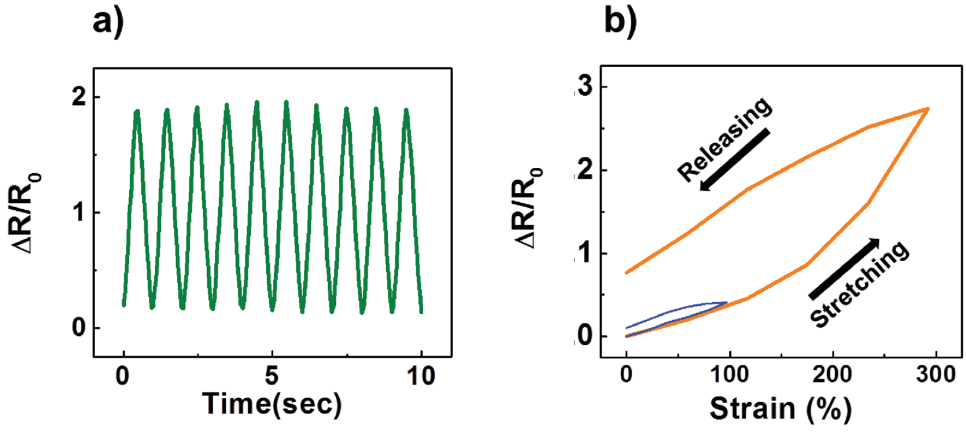


**Figure 5.** a) Relative change in resistance for cyclic strains between 0 and 300%. b) Hysteresis at 100% (blue) and 300% (orange) strains.

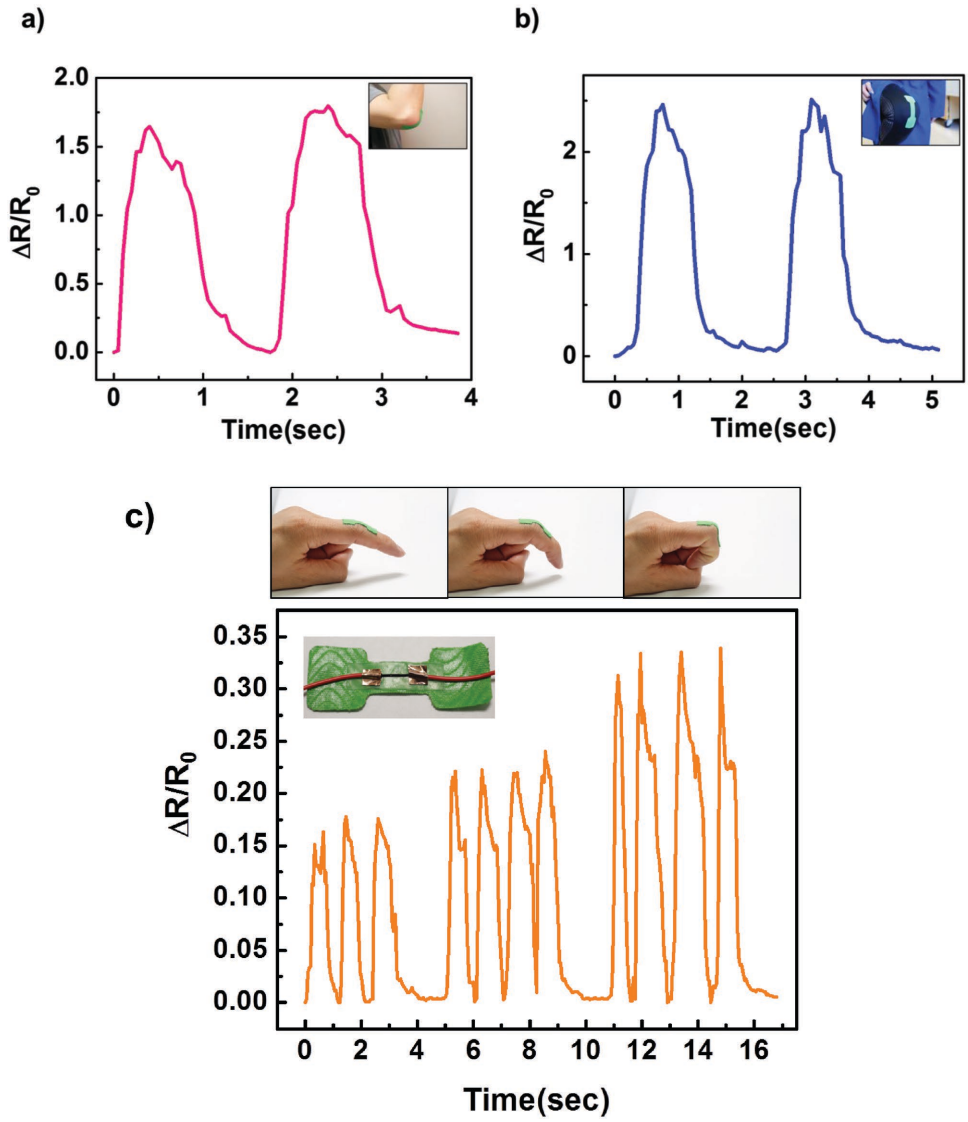


**Figure 6.** Wrinkled CNT-Ecoflex strain sensor was used to monitor human movement. Relative change in resistance while bending the strain sensor at joint area of a) elbow, b) knee, and c) finger.

the application of the sensors for detecting human motion by mounting the sensors onto the joint areas of the finger, elbow and knee. The maximum strain measured was ≈300%. This study suggests that these wCE sensors have applicability in a wide application range where measurements of large strains are required for physiological monitoring.

## Experimental Section

*Fabrication of Self-Similar Wrinkled CNT-Ecoflex Strain Sensor*: Initially, prestressed PS (KFS50-C, Grafix Arts) was rinsed with ethanol followed by deionized water. The sensor pattern was designed with CAD software (Autodesk, Inc., CA) and patterned on adhesive polymer film (Frisket Film, Grafix Arts). The pattern was subsequently cut with laser cutter (VLS2.30, Universal Laser Systems, AZ) and placed patterned adhesive polymer film, as a shadow mask, on top of a PS substrate. Spray gun method is used for deposit CNT solution (Aldrich) to the masked PS substrate. For the spray gun, the atomize nozzle and 0.5 mm tip size is used, the pressure was kept below 0.5 bar and the distance between spray gun and masked PS substrate is 25 cm for uniformity of CNT thin film deposition. The dispersed fluid of CNT solution, was evaporated by heating on the hotplate (≈65 °C) while spray gunned. The thickness of the CNT thin film is 115 nm and could be controlled by the amounts of the spray gunned CNT solution and distance between the spray gun and the working substrate. The thickness of CNT will affect to the size and wavelength of wrinkles which will affect its stretchability. The patterned CNT thin film was rinsed with deionized water for 10 min to remove surfactant and organic residue and dried completely with $N_2$ gun and light heating. After removing of the patterned shadow mask film, the deposited CNT thin film was pressed by the roller. The sample was placed into a convection oven for heat approximately to 150 °C to induce biaxial shrinking and wrinkling into the CNT thin film. The sensor design was shrunk to 33% of initial size. After forming a self-similar wrinkle on CNT thin film, a platinum-catalyzed silicone elastomer (Ecoflex 0030, Smooth-On, PA) was poured and spin coated (Laurell Technologies Corporation) at 150 rpm for 40 s. After spin coating, shrunk sample was

placed under vacuum for 10 min to remove bubbles and cured overnight at room temperature. Cured sample was placed into an acetone bath (75 °C) for 30 min followed by a toluene bath (65 °C) 10 min to remove any residual PS then dry in air for 12 h.

*Structure Characterization and Sensing of Strain*: SEM (FEI Magellan 400 XHR) was performed for imaging the wrinkles, and CNTs. The samples were sputter coated with Ir prior to SEM imaging. Strain sensitivity of wrinkled CNT-Ecoflex sensors was measured by a custom-made semi-static tensile strain stretching apparatus. The apparatus was a leadscrew based linear actuator driven by a stepper motor (Figure 3a). To avoid mechanical failure and to withstand large deformations while maintaining high electrical conductivities, liquid metals such as eutectic gallium-indium (EGaIn) were used rather than solid materials. Sensor is fixed at 0% strain and resistance is measured by 30% strain increments until failure. For cycling measurement, the sensors where strained from 0% to 300% using a saw-tooth wave form on a computer controlled linear strain testing apparatus. The resistance was sampled at 2 Hz with a multimeter connected to a computer. The samples were cycled over 1000 times at 2 Hz.

*Detecting the Human Motion (Finger, Elbow, and Knee)*: The wrinkled CNT-Ecoflex sensor was assembled on an elastic sports fitness tape to hold all the components together (Figure 6c inset). Measurements were taken using the same data acquisition system as previously mentioned.

*Finite Element Analysis*: FEA was performed to examine the strain and stress distribution in the Ecoflex and CNT film respectively. The models were created using Ansys DesignModeler, and analysis was performed with Ansys Workbench 16.0. The Ecoflex was modeled as a two parameter Mooney-Rivlin hyperleastic material,[65] and the carbon nanotube film was modeled as an isotropic elastic material. The stiffness of the carbon nanotube film was calculated using the wrinkle wavelength equation used by Fu et al.[66] To examine the distribution of normal stress within the carbon nanotube film, a simplified 2D model was created based off of SEM cross-section images of the of the transferred carbon nanotube sensor. The model was strained to 300% strain. To assess the normal strain distribution within the Ecoflex, three different Ecoflex geometries (rectangular, dumbbell, and hourglass) were modeled; each geometry was taken to 425% strain.

## Supporting Information

Supporting Information is available from the Wiley Online Library or from the author.

## Acknowledgements

The National Institute of Health (NIH) Director's New Innovator Award Program (1DP2OD007283).

Received: March 31, 2016
Revised: April 24, 2016
Published online:

[1] N. Lu, C. Lu, S. Yang, J. Rogers, *Adv. Funct. Mater.* **2012**, *22*, 4044.
[2] S. Luo, T. Liu, *Adv. Mater.* **2013**, *25*, 5650.
[3] F. Axisa, P. M. Schmitt, C. Gehin, G. Delhomme, E. Mcadams, A. Dittmar, *IEEE Trans. Inf. Technol. Biomed.* **2005**, *9*, 325.
[4] M. Sung, C. Marci, A. Pentland, *J. Neuroeng. Rehabil.* **2005**, *2*, 21.
[5] J. Hwang, J. Jang, K. Hong, K. N. Kim, J. H. Han, K. Shin, C. E. Park, *Carbon* **2011**, *49*, 106.
[6] J. Zhang, J. Liu, R. Zhuang, E. Mäder, G. Heinrich, S. Gao, *Adv. Mater.* **2011**, *23*, 3392.
[7] R. C. Webb, A. P. Bonifas, A. Behnaz, Y. Zhang, K. J. Yu, H. Cheng, M. Shi, Z. Bian, Z. Liu, Y.-S. Kim, W.-H. Yeo, J. S. Park, J. Song, Y. Li, Y. Huang, A. M. Gorbach, J. A. Rogers, *Nat. Mater.* **2013**, *12*, 938.
[8] G. Schwartz, B. C.-K. Tee, J. Mei, A. L. Appleton, D. H. Kim, H. Wang, Z. Bao, *Nat. Commun.* **2013**, *4*, 1859.
[9] B. Hu, W. Chen, J. Zhou, *Sens. Actuators, B* **2013**, *176*, 522.
[10] M. Hempel, D. Nezich, J. Kong, M. Hofmann, *Nano Lett.* **2012**, *12*, 5714.
[11] L. Persano, C. Dagdeviren, Y. Su, Y. Zhang, S. Girardo, D. Pisignano, Y. Huang, J. A. Rogers, *Nat. Commun.* **2013**, *4*, 1633.
[12] H. Vandeparre, D. Watson, S. P. Lacour, *Appl. Phys. Lett.* **2013**, *103*, 2.
[13] Y. Qi, J. Kim, T. D. Nguyen, B. Lisko, P. K. Purohit, M. C. McAlpine, *Nano Lett.* **2011**, *11*, 1331.
[14] D.-Y. Khang, H. Jiang, Y. Huang, J. A. Rogers, *Science* **2006**, *311*, 208.
[15] S. P. Lacour, D. Chan, S. Wagner, T. Li, Z. Suo, *Appl. Phys. Lett.* **2006**, *88*, 1.
[16] M. Zheng, W. Li, M. Xu, N. Xu, P. Chen, M. Han, B. Xie, *Nanoscale* **2014**, *6*, 3930.
[17] H. Wang, X. Han, X. Ou, C.-S. Lee, X. Zhang, S.-T. Lee, *Nanoscale* **2013**, *5*, 8172.
[18] K. Takei, T. Takahashi, J. C. Ho, H. Ko, A. G. Gillies, P. W. Leu, R. S. Fearing, A. Javey, *Nat. Mater.* **2010**, *9*, 821.
[19] X. Xiao, L. Yuan, J. Zhong, T. Ding, Y. Liu, Z. Cai, Y. Rong, H. Han, J. Zhou, Z. L. Wang, *Adv. Mater.* **2011**, *23*, 5440.
[20] A. B. Dalton, S. Collins, E. Muñoz, J. M. Razal, V. H. Ebron, J. P. Ferraris, J. N. Coleman, B. G. Kim, R. H. Baughman, *Nature* **2003**, *423*, 703.
[21] Q. Fan, Z. Qin, S. Gao, Y. Wu, J. Pionteck, E. Mäder, M. Zhu, *Carbon* **2012**, *50*, 4085.
[22] D. J. Lipomi, M. Vosgueritchian, B. C.-K. Tee, S. L. Hellstrom, J. A. Lee, C. H. Fox, Z. Bao, *Nat. Nanotechnol.* **2011**, *6*, 788.
[23] F. Mirri, A. W. K. Ma, T. T. Hsu, N. Behabtu, S. L. Eichmann, C. C. Young, D. E. Tsentalovich, M. Pasquali, *ACS Nano* **2012**, *6*, 9737.
[24] Y. Shang, X. He, Y. Li, L. Zhang, Z. Li, C. Ji, E. Shi, P. Li, K. Zhu, Q. Peng, C. Wang, X. Zhang, R. Wang, J. Wei, K. Wang, H. Zhu, D. Wu, A. Cao, *Adv. Mater.* **2012**, *24*, 2896.
[25] T. Yamada, Y. Hayamizu, Y. Yamamoto, Y. Yomogida, A. Izadi-Najafabadi, D. N. Futaba, K. Hata, *Nat. Nanotechnol.* **2011**, *6*, 296.
[26] S. Tadakaluru, W. Thongsuwan, P. Singjai, *Sensors* **2014**, *14*, 868.
[27] S. H. Bae, Y. Lee, B. K. Sharma, H. J. Lee, J. H. Kim, J. H. Ahn, *Carbon* **2013**, *51*, 236.
[28] H. Tian, Y. Shu, Y. Cui, W. Mi, Y. Yang, T. Ren, *Nanoscale* **2014**, 699.
[29] H. Tian, Y. Shu, Y.-L. Cui, W.-T. Mi, Y. Yang, D. Xie, T.-L. Ren, *Nanoscale* **2014**, *6*, 699.
[30] Y. Wang, L. Wang, T. Yang, X. Li, X. Zang, M. Zhu, K. Wang, D. Wu, H. Zhu, *Adv. Funct. Mater.* **2014**, *24*, 4666.
[31] K. S. Kim, Y. Zhao, H. Jang, S. Y. Lee, J. M. Kim, K. S. Kim, J.-H. Ahn, P. Kim, J.-Y. Choi, B. H. Hong, *Nature* **2009**, *457*, 706.
[32] D. Kang, P. V. Pikhitsa, Y. W. Choi, C. Lee, S. S. Shin, L. Piao, B. Park, K.-Y. Suh, T. Kim, M. Choi, *Nature* **2014**, *516*, 222.
[33] X. Li, R. Zhang, W. Yu, K. Wang, J. Wei, D. Wu, A. Cao, Z. Li, Y. Cheng, Q. Zheng, R. S. Ruoff, H. Zhu, *Sci. Rep.* **2012**, *2*, 870.
[34] C. Yan, J. Wang, W. Kang, M. Cui, X. Wang, C. Y. Foo, K. J. Chee, P. S. Lee, *Adv. Mater.* **2014**, *26*, 2022.
[35] A. V. Zaretski, S. E. Root, A. Savchenko, E. Molokanova, A. D. Printz, L. Jibril, G. Arya, M. Mercola, D. J. Lipomi, *Nano Lett.* **2016**, *16*, 1375.
[36] R. H. Baughman, A. A. Zakhidov, W. A. de Heer, *Science* **2002**, *297*, 787.
[37] S. J. Tans, M. H. Devoret, H. Dai, A. Thess, R. E. Smalley, L. J. Geerligs, C. Dekker, *Nature* **1997**, *386*, 474.
[38] R. S. Ruoff, D. C. Lorents, *Carbon* **1995**, *33*, 925.
[39] M. M. J. Treacy, T. W. Ebbesen, J. M. Gibson, *Nature* **1996**, *381*, 678.
[40] M. H. Andrew Ng, L. T. Hartadi, H. Tan, C. H. Patrick Poa, *Nanotechnology* **2008**, *19*, 205703.

[41] J. M. Harris, G. R. S. Iyer, A. K. Bernhardt, J. Y. Huh, S. D. Hudson, J. A. Fagan, E. K. Hobbie, *ACS Nano* **2011**, *6*, 881.
[42] S. Ryu, P. Lee, J. B. Chou, R. Xu, R. Zhao, A. J. Hart, S. Kim, *ACS Nano* **2015**, *9*, 5929.
[43] J. Lu, M. Lu, A. Bermak, S. Member, Y. Lee, in *Proc. 7th IEEE Int. Conf. Nanotechnology (IEEE-NANO)* (Ed: Heidi Y. Y. Wong), IEEE, Piscataway, NJ, USA **2007**, 1240.
[44] M. Amjadi, A. Pichitpajongkit, S. Lee, S. Ryu, I. Park, *ACS Nano* **2014**, *8*, 5154.
[45] S. Gong, W. Schwalb, Y. Wang, Y. Chen, Y. Tang, J. Si, B. Shirinzadeh, W. Cheng, *Nat. Commun.* **2014**, *5*, 1.
[46] S. Luo, T. Liu, *Carbon* **2013**, *59*, 315.
[47] D.-H. Kim, N. Lu, R. Ma, Y.-S. Kim, R.-H. Kim, S. Wang, J. Wu, S. M. Won, H. Tao, A. Islam, K. J. Yu, T. Kim, R. Chowdhury, M. Ying, L. Xu, M. Li, H.-J. Chung, H. Keum, M. McCormick, P. Liu, Y. Zhang, F. G. Omenetto, Y. Huang, T. Coleman, J. A. Rogers, *Science* **2011**, *333*, 838.
[48] X. Liu, Y. Zhu, M. W. Nomani, X. Wen, T.-Y. Hsia, G. Koley, *J. Micromech. Microeng.* **2013**, *23*, 025022.
[49] S. Ryu, P. Lee, J. B. Chou, R. Xu, R. Zhao, A. J. Hart, S. Kim, *ACS Nano* **2015**, 5929.
[50] F. Xu, Y. Zhu, *Adv. Mater.* **2012**, *24*, 5117.
[51] J. K. Paik, R. K. Kramer, R. J. Wood, *IEEE Int. Conf. Intelligent Robotics and Systems*, (Ed: Oussama Khatib), IEEE, Piscatawy, NJ, USA **2011**, 414.
[52] J. D. Pegan, A. Y. Ho, M. Bachman, M. Khine, *Lab Chip* **2013**, *13*, 4205.
[53] S. Lin, E. K. Lee, N. Nguyen, M. Khine, *Lab Chip* **2014**, *14*, 3475.
[54] R. C. Tenent, T. M. Barnes, J. D. Bergeson, A. J. Ferguson, B. To, L. M. Gedvilas, M. J. Heben, J. L. Blackburn, *Adv. Mater.* **2009**, *21*, 3210.
[55] C. Preston, D. Song, J. Dai, Z. Tsinas, J. Bavier, J. Cumings, V. Ballarotto, L. Hu, *Nano Res.* **2015**, *8*, 2242.
[56] J. Kim, S.-J. Park, T. Nguyen, M. Chu, J. D. Pegan, M. Khine, *Appl. Phys. Lett.* **2016**, *108*, 061901.
[57] W. S. Bao, S. A. Meguid, Z. H. Zhu, G. J. Weng, W. S. Bao, S. A. Meguid, Z. H. Zhu, G. J. Weng, *J. Appl. Phys.* **2014**, *111*, 093726.
[58] N. Hu, Y. Karube, C. Yan, Z. Masuda, H. Fukunaga, *Acta Mater.* **2008**, *56*, 2929.
[59] C. Li, E. T. Thostenson, T. W. Chou, *Appl. Phys. Lett.* **2007**, *91*, 223114.
[60] O. Kanoun, C. Müller, A. Benchirouf, A. Sanli, T. N. Dinh, A. Al-Hamry, L. Bu, C. Gerlach, A. Bouhamed, *Sensors* **2014**, *14*, 10042.
[61] Y. Y. Hsu, M. Gonzalez, F. Bossuyt, J. Vanfleteren, I. De Wolf, *IEEE Trans. Electron Devices* **2011**, *58*, 2680.
[62] J. A. Fan, W.-H. Yeo, Y. Su, Y. Hattori, W. Lee, S.-Y. Jung, Y. Zhang, Z. Liu, H. Cheng, L. Falgout, M. Bajema, T. Coleman, D. Gregoire, R. J. Larsen, Y. Huang, J. A. Rogers, *Nat. Commun.* **2014**, *5*, 3266.
[63] C. F. Guo, T. Sun, Q. Liu, Z. Suo, Z. Ren, *Nat. Commun.* **2014**, *5*, 1.
[64] M. Leser, J. Pegan, M. El Makkaoui, J. C. Schlatterer, M. Khine, M. Law, M. Brenowitz, *Lab Chip* **2015**, *15*, 1381.
[65] Y. Huang, Y. Wang, L. Xiao, H. Liu, W. Dong, Z. Yin, *Lab Chip* **2014**, *14*, 4205.
[66] C. C. Fu, A. Grimes, M. Long, C. G. L. Ferri, B. D. Rich, S. Ghosh, S. Ghosh, L. P. Lee, A. Gopinathan, M. Khine, *Adv. Mater.* **2009**, *21*, 4472.